TRENDS IN SCIENCES 2026; 23(12): 14097
https://doi.org/10.48048/tis.2026.14097 RESEARCH ARTICLE

Extraction of Coconut Coir-Derived Lignin and Fabrication of Electrospun Nanofibers of Nylon 6/Lignin Blends

Supapohn Pohnanothai and Patcharaporn Wutticharoenmongkol*

Department of Chemical Engineering, Faculty of Engineering, Thammasat School of Engineering, Thammasat University, Pathumthani 12120, Thailand

(*Corresponding author's e-mail: tpatchar@engr.tu.ac.th)

Received: 14 April 2026, Revised: 22 May 2026, Accepted: 2 June 2026, Published: 20 July 2026

Abstract

This research introduces a sustainable and integrated approach for utilizing lignin derived from coconut coir, employing a deep eutectic solvent (DES) system to synthesize advanced nanofibers. The study methodically optimized lignin extraction, emphasizing yield, antioxidant capacity, structural attributes (as determined by FTIR and XRD analyses), and antibacterial efficacy. The optimal extraction parameters were established as 80 °C for a duration of 8 h (C80–8). Consequently, this methodology achieved the highest lignin recovery rate (15.95%), while simultaneously maintaining the inherent structural integrity and mitigating condensation. Structural analyses confirmed the retention of critical functional groups and a largely amorphous configuration. The C80–8 lignin demonstrated enhanced antioxidant activity (IC50 = 30 µg/mL) and exhibited significantly improved antibacterial efficacy against both Staphylococcus aureus and Escherichia coli, in contrast to Kraft lignin (KL). Following this, the extracted lignin was integrated into a Nylon 6 matrix and subsequently processed into composite nanofibers via needleless electrospinning. The impact of lignin loading was methodically evaluated through morphological and mechanical characterization. SEM analysis revealed that a 5 wt% lignin loading (N/CL5) produced uniform, bead-free nanofibers with an average diameter of 104 nm, indicating that the conditions for rheology and electrospinning were appropriately optimized. This formulation also had the best mechanical properties, with higher tensile strength, elongation at break, and Young's modulus. The observed results arose from the interactions between lignin and the polymer matrix, specifically the formation of hydrogen bonds. Furthermore, the N/CL5 nanofibers showed significant antibacterial activity against S. aureus, surpassing the effectiveness of both pure Nylon 6 and KL composites. The enhanced functionality of DES-extracted lignin is due to the large number of phenolic hydroxyl groups that were preserved. The findings generally indicate that lignin derived from DES offers two key advantages: Its potential as a reinforcing agent and its utility as a bioactive additive. Consequently, this approach presents a scalable and environmentally sound method for converting lignocellulosic agricultural waste into valuable materials suitable for biomedical, protective, and filtration applications.

Keywords: Lignin, Coconut coir, Deep eutectic solvent (DES), Nylon 6, Needleless electrospinning

Introduction

The increasing global demand for renewable and sustainable resources has significantly enhanced research on utilizing lignocellulosic biomass derived from agricultural waste. As a highly viable alternative feedstock, lignocellulosic biomass presents enormous potential to produce value-added materials, intermediate chemicals, and biofuels. This biomass source is renewable, abundant, and has a natural hierarchical structure. It's mainly made up of three large molecular components: Cellulose, hemicellulose, and lignin [1]. Thailand is a tropical region with a lot of agricultural residues, particularly from coconuts (*Cocos nucifera* L.). While the commercial coconut industry mainly uses water and fresh by-products like coconut coir, the mesocarp or outer husk is often discarded. Unfortunately, this valuable lignocellulosic fiber is

frequently disposed of through open burning or landfilling, causing environmental harm [2]. Coconut coir is often thought of as waste, but it has a high lignin content, as well as cellulose and hemicellulose, making it a promising and underused resource for the production of bioenergy, biochemicals, and advanced biobased functional materials [3].

Lignin is the second most common natural polymer on Earth, following cellulose. It makes up about 10% to 25% of the total amount of lignocellulosic biomass. Lignin is a three-dimensional, cross-linked, and amorphous macromolecule made up of phenolic monomers. This produces an extremely complex and recalcitrant structural network with numerous functional groups and chemical links [4]. Because of its unique molecular architecture, lignin has a wide range of remarkable properties, including exceptional antioxidant capacity, potent antimicrobial and antibacterial activities, excellent UV-shielding capabilities, and strong thermal resistance. These versatile properties have recently gained attention in a variety of industries due to their potential applications in biocomposites, protective coatings, high-performance adhesives, and advanced biomedical materials [5,6]. However, efficiently utilizing and extracting lignin presents a difficult challenge. The lignin macromolecule features a complex and tightly bound structure, along with holocellulose, which complicates access and separation. Consequently, a pretreatment process is necessary to destroy the biomass matrix and improve its accessibility [7]. At present, traditional pretreatment and extraction techniques encounter significant constraints in terms of high energy consumption, operational costs, and degradation of biomass [8]. To address these ongoing extraction challenges, Deep Eutectic Solvents (DES) have emerged as highly effective, environmentally friendly solvent technologies that have received significant scientific attention. DES systems have numerous advantages over traditional lignin extraction methods [9]. These advantages include the ability to dissolve lignin, low vapor pressure, high biodegradability, and simple synthesis protocols. In addition, DES systems typically include hydrogen bond donors (HBDs) and acceptors (HBAs). The exact combinations and molar ratios of these components can be precisely adjusted to target specific types of biomass. This makes DES a very flexible and environmentally friendly way to get the most lignin back without hurting its molecular structure or losing its useful properties [10].

The blending of polymers with recovered lignin, following sustainable extraction methods, presents a promising opportunity to create high-value advanced materials. In this context, the production of lignin-reinforced composite nanofibers using electrospinning technology has gained significant attention. Electrospinning is an efficient and versatile method for producing ultrafine fibers that are thinner, more uniform, and possess higher surface-area-to-volume ratios, along with adjustable porosity compared to other techniques [11]. This process utilizes strong electrostatic forces to transform custom polymer solutions into long, thin strands that are only a few microns wide. This occurs when a strong electric field is present [12]. Previous studies have shown that combining lignin with other materials can be effective. For instance, electrospun fibers containing lignin and poly(ethylene terephthalate) (PET) were more water-loving and had strong antibacterial and antiviral properties [13]. Lignin-based films combined with chitosan are effective for long-term food packaging due to their strong antioxidant and antimicrobial properties [14]. Although traditional electrospinning methods are effective, their reliance on single-needle configurations inherently limits production rates and leads to operational issues such as needle clogging. In contrast, needleless electrospinning offers a high-capacity solution to manufacturing challenges by significantly increasing nanofiber productivity through the simultaneous formation of multiple polymeric jets from a free liquid surface. As a result, yields can be 3 to 250 times higher than those of traditional needle-based systems, while also eliminating the frustrating issue of needle occlusion during continuous processing [15]. Nylon 6 nanofiber membranes are widely studied for their high mechanical strength, porosity, and surface area, and are typically produced using traditional spinning techniques like melt, spinning, and wet spinning, demonstrating strong potential across various applications [16].

However, despite the progress in biomass pretreatment technologies, significant knowledge gaps remain. Previous studies have demonstrated the effectiveness of DES in lignin extraction and

valorization [17]. Nevertheless, comprehensive studies focusing on the yield and molecular structure of lignin derived specifically from coconut coir are still limited. Furthermore, although lignin-based polymer composites have been widely explored [18]. Their integration into Nylon 6 nanocomposites via highly scalable needleless electrospinning remains underexplored, particularly in terms of process scalability and functional performance. Integrating synergistically is crucial for creating efficient and sustainable products, such as advanced absorbent membranes and wound dressings.

This research aims to develop a comprehensive and sustainable process for valorizing coconut coir using a circular bioeconomy approach. First, lignin will be extracted using an optimized DES system and evaluated in terms of yield, structural characteristics, and bio-functional properties. Second, Nylon 6/lignin composite nanofibers will be fabricated using a needleless electrospinning technique to overcome the scalability limitations of conventional systems. Finally, the morphological, mechanical, and antibacterial properties of the resulting nanofiber mats will be systematically evaluated. Ultimately, this research showcases a highly scalable strategy that effectively converts underutilized agricultural waste into high-performance functional nanomaterials for a diverse range of advanced applications.

Materials and methods

Material and chemical

The following chemicals and reagents were used in this study. Coconut coir was obtained from Phetchabun Province, Thailand. Nylon-6 (polycaprolactam) pellets and 2,2-diphenyl-1-picrylhydrazyl (DPPH) were purchased from Sigma-Aldrich (Germany). Alkali kraft lignin (KL) was obtained from Sigma-Aldrich (USA). Choline chloride (≥ 98%, extra pure) and lactic acid (88%, analytical reagent grade) were supplied by Loba Chemie (India). Formic acid (90%) was purchased from KEMAUS (Australia), while acetone (≥ 99.5%) was obtained from RCI Labscan Limited (Thailand). *N, N*-dimethylformamide (DMF) was purchased from Carlo Erba Reagents (France). Deionized water was used throughout all experiments. All reagents were used as received without further purification. Unless otherwise specified, all solvents were of analytical reagent grade.

Extraction of lignin

Coconut coir was washed, dried, milled, and sieved to obtain 40 mesh powder. The material was oven-dried at 60 °C for 24 h before use. DES was prepared by mixing choline chloride and lactic acid at a 1:5 molar ratio, modified from Kumar *et al*. [19], and heating at 60 °C in a shaking water bath (100 rpm) until a clear homogeneous liquid formed.

Pretreatment was conducted using a full factorial design comprising three temperatures and three reaction times. Extraction was performed at 60, 70, and 80 °C for 8, 12, and 16 h at a biomass-to-DES ratio of 1:10 (w/v) under agitation (100 rpm), resulting in nine experimental conditions. The experimental conditions are summarized in **Table 1**. The solid fraction was separated by vacuum filtration using a 1 µm membrane. Lignin was precipitated by adding distilled water to the filtrate and stored at 4 °C for 12 h. The precipitate was collected by centrifugation (5000 rpm for 30 min), washed until the pH was neutral, and dried at 70 °C for 12 h before analysis. The lignin yield was calculated based on the initial lignin content of coconut coir (32.1%), as reported by Rencoret *et al.* [20]. All experiments were performed in triplicate (n = 3), and the results are expressed as mean ± standard deviation (SD). The DES-water mixture was recovered by rotary evaporation.

Fourier transform infrared (FTIR) analysis of lignin

FTIR spectra were recorded using a PerkinElmer (USA) spectrometer to identify the functional groups present in the extracted lignin sample. Samples were dried at 105 °C for 3 - 5 h before measurement. Spectra were collected over the range of 4,000 - 400 cm^{-1} using an attenuated total reflectance (ATR) accessory, with 64 scans per sample at a resolution of 4 cm^{-1}.

X-ray diffraction (XRD) analysis of lignin

XRD analysis was performed to evaluate the crystallinity of powdered lignin samples extracted from coconut coir using an X-ray diffractometer (MiniFlex600-C, Rigaku, Japan). The instrument was operated under θ - 2θ geometry with Cu-Kαl filter radiation at 30 kV and 30 mA. Diffraction patterns were

recorded in a 2θ range from 10° to 70° at a scanning speed of 2°/min.

Antioxidant activity analysis of lignin

The DPPH radical-scavenging assay was performed according to the methods described by Rumpf *et al.* [21], with minor modifications. A 0.25 mM DPPH solution was prepared in methanol, and lignin samples were dissolved in DMF at concentrations of 0.02 - 1.0 mg mL^{-1}. An aliquot of 120 µL of lignin solution was mixed with 4.5 mL of DPPH solution and incubated in the dark at room temperature for 30 min. The absorbance was measured at 517 nm using a UV-Vis spectrophotometer (UV-5100, Metash, China). Measurements were performed in triplicate. Radical scavenging activity was calculated using Eq. (1). The calculated IC_{50} value represents the concentration required to inhibit 50% of the initial DPPH radicals, illustrating the compound's efficacy in scavenging free radicals.

$$\text{DPPH radical scavenging assay (\%)} = \frac{A_{\text{control}} - A_{\text{sample}}}{A_{\text{control}}} \times 100 \quad (1)$$

A_{control}= absorbance of the control solution (DPPH + DMF), and A_{sample}= absorbance of the sample solution (DPPH + lignin solution). IC_{50} values were determined by linear regression [22]. All experiments were performed in triplicate (n = 3), and data are presented as mean ± SD.

Antibacterial activity analysis of lignin

The agar disk diffusion assay evaluated antibacterial activity according to Gordobil *et al.* [23]. *Escherichia coli (E. coli)* ATCC 25922 and *Staphylococcus aureus (S. aureus)* ATCC 25923 were adjusted to 0.5 McFarland standard and swabbed onto Mueller-Hinton agar plates. Sterile filter paper disks (6 mm) impregnated with lignin solution (0.02 g mL^{-1}, dissolved in Dimethyl Sulfoxide, DMSO) were placed on the inoculated plates. Disks containing DMSO were used as negative controls. After incubation at 35 °C for 16 - 18 h, inhibition zones were measured and expressed as mean diameter (mm) ± SD (n = 3).

Preparation and characterization of Nylon 6/lignin blends solutions

Nylon-6 was first dissolved in formic acid to obtain a 15% (w/v) solution under magnetic stirring at 200 rpm for approximately 3 h until completely dissolved. Subsequently, lignin powder was added to the Nylon-6 solution at 0, 2.5, 5, and 7.5 wt%, calculated relative to the mass of Nylon-6 present in the solution. The mixtures were further stirred for 3 h to ensure complete dispersion and homogeneity before electrospinning and characterization. The detailed compositions of each solution are summarized in **Table 1**. Due to the high polymer content, a slight temperature increase was observed during stirring. Therefore, all measurements were conducted within 24 h after solution preparation to ensure thermal equilibrium and complete homogenization. Each formulation was prepared freshly before electrospinning, and the experiments were conducted in triplicate to minimize aging effects and preparation variability.

The kinematic viscosity of the solutions was measured at 40 °C using a Cannon-Fenske Routine viscometer (size 450, viscometer constant = 2.486 $mm^2 s^{-2}$) in accordance with ASTM D2162. Electrical conductivity was measured at 25 °C using a Lutron CD-4318SD conductivity meter. Surface tension was determined at 25 °C using a contact angle goniometer (DataPhysics OCA 25) equipped with a pendant drop analysis system. All solution samples were performed in triplicate (n = 3), and data are presented as mean ± SD.

Table 1 The compositions of Nylon 6/lignin blend samples.

Sample code	Lignin type	Lignin concentration (w/w)
N/L0	-	0
N/CL2.5	Coconut coir lignin (selected condition)	2.5
N/CL5		5
N/CL7.5		7.5
N/KL2.5	Kraft Lignin (KL)	2.5
N/KL5		5
N/KL7.5		7.5

Needleless electrospinning process

The electrospinning process was performed using a Nanospider LAB laboratory setup (Elmarco, Czech Republic) equipped with a string electrode. A polypropylene spunbonded material was used as the substrate, and the distance between the electrodes was fixed at 140 mm. All solutions were electrospun at an applied voltage of 70 kV under a relative humidity of 40%. The selected voltage was based on the operational parameters of the Nanospider system and previous studies reported by Aulova *et al.* [24]. A 10 mL portion of the Nylon 6/lignin solution was loaded into the container and positioned appropriately relative to the string electrode. The resulting nanofiber mats were collected on the substrate and subsequently stored in a desiccator before further characterization.

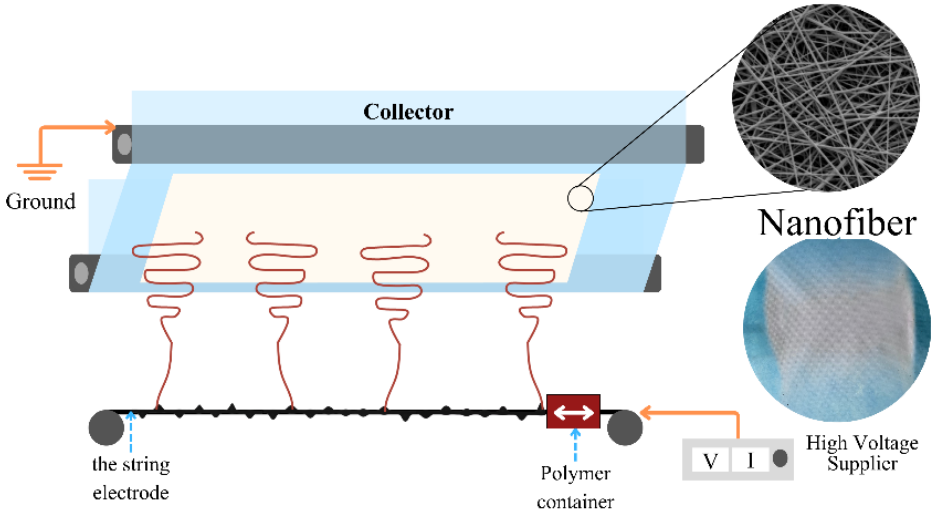


Figure 1 Schematic diagram of needleless electrospinning using a string electrode to produce a nanofiber mat.

Morphological characterization of nanofiber mats

The morphology of electrospun nanofiber mats was examined by a field emission scanning electron microscope (FE-SEM, JEOL JSM7800F, Japan). Each specimen was Au-coated using a QUORUM Q150R ES (United Kingdom) sputtering device before being observed under the SEM with a magnification of 15000×. For each spinning condition, 100 measurements of the fiber diameter were recorded by image-analysis software (ImageJ version 1.54). Statistical analysis of the data obtained was carried out by constructing a histogram, from which an arithmetic mean ± SD (n = 100) was obtained and reported.

The average fiber diameter was calculated, and the fiber diameter distribution width was determined using the fiber diameter uniformity coefficient, which is the ratio of the weight average (A_w) to the number average (A_n) optimum value should be very close to 1 for uniform fibers [25]. Following Eqs. (2) and (3):

$$\text{The uniformity efficient } = \frac{A_w}{A_n} \quad (2)$$

where

$$A_n = \frac{\Sigma n_i d_i}{\Sigma n_i}, A_n = \frac{\Sigma n_i d_i^2}{\Sigma n_i d_i} \quad (3)$$

d_i: fiber diameter and n_i : Number of fibers

Mechanical tests of nanofiber mats

The mechanical properties of the nanofiber mats were evaluated in accordance with ASTM D882 using a universal testing machine (UTM) to determine tensile strength and elongation at break. Specimens with a width of 20 mm and a gauge length of 50 mm were tested at a crosshead speed of 5 mm min^{-1}. The thickness of each specimen was measured at five positions with a digital micrometer, and the average was used in the calculations. Tensile strength and elongation at break were calculated using Eqs. (4) and (5), respectively.

$$\text{Tensile strength} = \frac{F_{max}}{w \times t} \quad (4)$$

where F_{max} is the maximum load (N), w is the specimen width (mm), and t is the average thickness (mm).

$$\text{Elongation at break} = \frac{\Delta L}{L_0} \times 100 \quad (5)$$

where ΔL is the extension at break (mm) and L_0 is the initial gauge length (50 mm).

Antibacterial activity of nanofiber mats (agar disk diffusion assay)

The samples were tested using the same procedure as described previously for the antibacterial activity (Antibacterial activity analysis of lignin). Nanofiber mat samples were cut into 6 mm diameter circular discs and placed onto the inoculated plates. A nanofiber mat without the addition of lignin was used as the negative control. After incubation at 35 °C for 16 - 18 h, the inhibition zones were measured, and all solution samples were performed in triplicate (n = 3).

Results and discussion

Optimum conditions for lignin extraction

The extraction of lignin from coconut coir under DES conditions at 60, 70, and 80 °C for 8, 12, and 16 h is summarized in **Table 2**. The optimal conditions for lignin extraction from coconut coir using DES solvent (choline chloride combined with lactic acid, 1:5 ratio) at 80°C for 8 h (Sample: C80-8) showed that temperature significantly influenced lignin yield more than extraction time. Increasing the temperature from 60 to 70 and 80 °C resulted in a significant increase in lignin recovery. This aligns with the role of temperature in reducing solvent viscosity and increasing mass transfer rate, allowing DES to penetrate and break down lignocellulose structures more efficiently. The DPPH radical scavenging activity of the extracted lignin increased with increasing lignin concentration, as shown in **Figure 2**. The calculated IC_{50} values from the DPPH assay indicate antioxidant potency, where lower IC_{50} values correspond to stronger radical scavenging activity. Under condition C80–8, not only was the highest yield (15.95%) achieved, but it also exhibited the best antioxidant activity with a low IC50 of only 30 µg/mL, clearly surpassing commercial kraft lignin. However, extending the extraction time to 12 and 16 h at the same temperature resulted in different yields. Both yield and antioxidant activity were found to decrease, with the IC50 increasing to 82 µg/mL at 16 h, reflecting structural degradation of lignin under harsh conditions. These results are consistent with the work of Mankar *et al*. [26], who found that while high temperatures can accelerate lignin extraction to high yields in a short time, prolonged extraction beyond the optimal point resulted in decreased yield due to structural changes in lignin and reprecipitation on the biomass surface. Furthermore, high heat accelerates carbohydrate degradation, interfering with the purity and extraction efficiency of lignin.

Table 2 Effect of temperature and time of DES extraction on lignin yield and antioxidant activity (IC_{50}).

Temperature (°C)	Time (h)	Sample code	Yield (%)	IC_{50} (µg/mL)
60	8	C60-8	4.75 ± 1.13	87 ± 4
	12	C60-12	5.22 ± 1.34	51 ± 3
	16	C60-16	5.25 ± 0.71	42 ± 5
70	8	C70-8	12.35 ± 0.99	64 ± 2
	12	C70-12	10.46 ± 1.35	52 ± 4
	16	C70-16	12.24 ± 1.22	35 ± 8
80	8	C80-8	15.95 ± 0.49	30 ± 6
	12	C80-12	10.93 ± 1.19	40 ± 1
	16	C80-16	7.50 ± 0.17	82 ± 1
Kraft Lignin		KL	-	140 ± 12

The C80-8 moderate condition exhibited the highest antioxidant efficiency, explained by the research of Duan *et al.* [27] and Alzagameem *et al.* [28], who concluded that the antioxidant activity of lignin varies with the amount of phenolic hydroxyl groups, low molecular weight, and narrow polydispersity. DES extraction under mild conditions effectively breaks down ether bonds in the lignin-carbohydrate complex (LCC), resulting in smaller lignin molecules rich in phenolic groups ready to donate protons for free radical scavenging. Conversely, overly harsh conditions can hinder this process. Lignin undergoes condensation, resulting in larger molecules that hinder chemical reactions and ultimately lose their antioxidant potential [10]. According to Agrawal *et al*. [29], who evaluated sustainable coconut coir extraction strategies using DES, indicates that the advantage of the DES system is that choline chloride ions disrupt the interaction between lignin and carbohydrates, while organic acids such as lactic acid cleave chemical bonds. This allows for the recovery of lignin in its native form, maintaining its hydrophobic properties without the need for harsh acidic or alkaline conditions that damage the polymer structure.

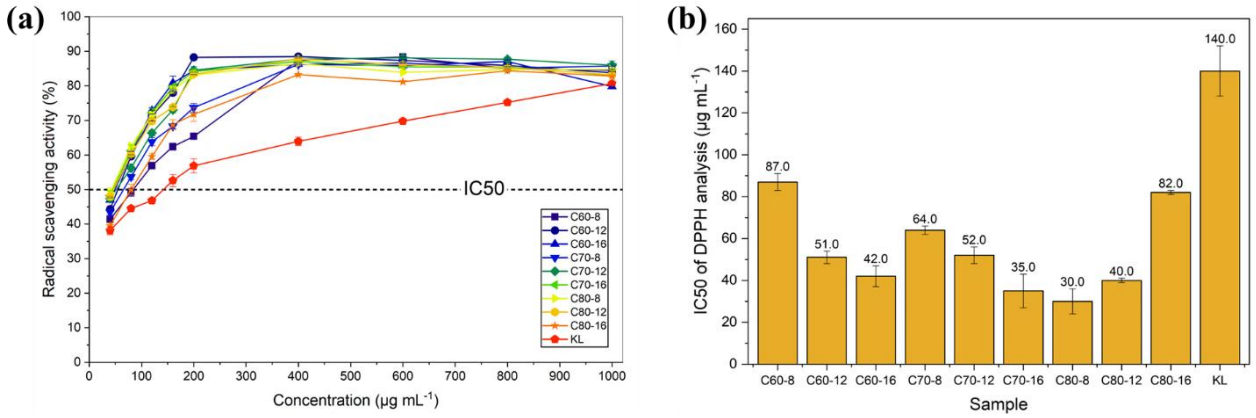


Figure 2 (a) DPPH radical scavenging activity and (b) IC_{50} of DPPH analysis of lignin extracted from various conditions.

Characterizations of lignin

The FTIR spectra of extracted lignin and kraft lignin recorded in the range of 4,000 - 400 cm^{-1} are presented in **Figure 3**. The spectra reveal multiple characteristic absorption bands, reflecting the structural complexity of lignin. The strong similarity between the extracted lignin and kraft lignin indicates that DES extraction effectively isolated lignin while preserving its aromatic backbone structure.

Consistent with previous reports [27,28], the broad band at 3,335 cm^{-1} corresponds to O–H stretching (phenolic and aliphatic hydroxyl groups), while peaks at 2,935 - 2,918 and 2,850 - 2,840 cm^{-1} are assigned to C–H stretching in methyl groups. The band at 1,726 cm^{-1} is attributed to C=O stretching. Characteristic aromatic skeletal vibrations appear at 1,600 - 1,500 cm^{-1} and 1,422 cm^{-1}. Peaks at 1,452 - 1,440 cm^{-1} are related to C–H deformation of methyl groups, and the band at 1370 cm^{-1} is associated with phenolic O–H and syringyl units. Signals at 1,273 - 1,265 and 1,210 cm^{-1} correspond to syringyl (S) units, whereas the peak at 1,120 cm^{-1} is characteristic of guaiacyl (G) units. The bands at 1,040 - 1,028 cm^{-1} are attributed to primary alcohol O–H stretching, and the peaks at 854 - 820 cm^{-1} correspond to C–H out-of-plane vibrations of *p*-hydroxyphenyl (H) units. Furthermore, the absorption band at 3,335 cm^{-1} for CL is more intense than that of kraft lignin, indicating a higher concentration of hydroxyl groups in CL.

The XRD patterns in **Figure 4** show that C80–8 exhibits a broad diffraction peak centered at approximately $2\theta \approx 21°$, indicating the amorphous structure of the sample. This pattern is highly comparable to those of kraft lignin and the reference lignin reported by Gomide *et al.* [30], which displayed a maximum peak at $2\theta = 20.26°$, suggesting that the DES extraction did not significantly alter the intrinsic structural organization of lignin.

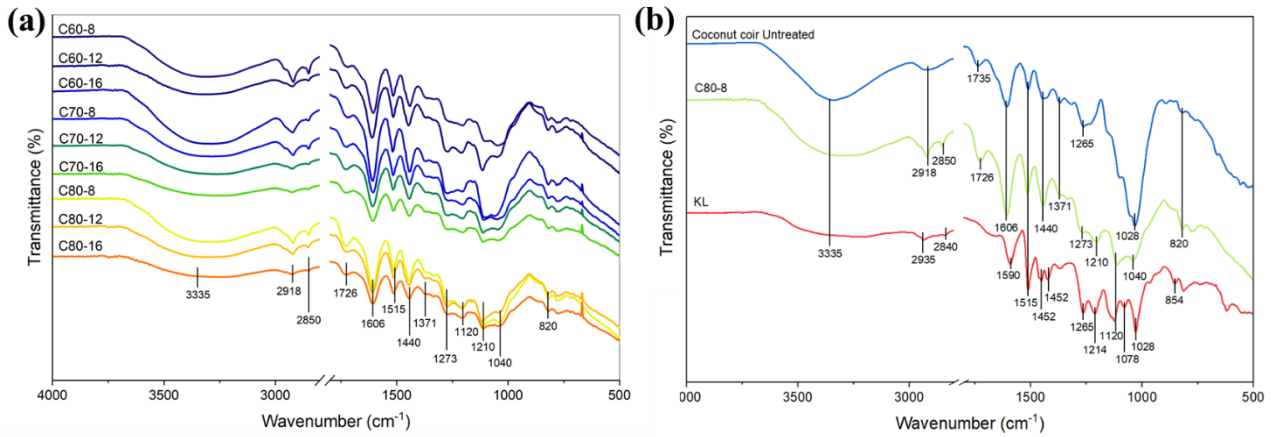


Figure 3 FTIR spectra of (a) all extracted lignin and (b) comparison between C80-8 and KL.

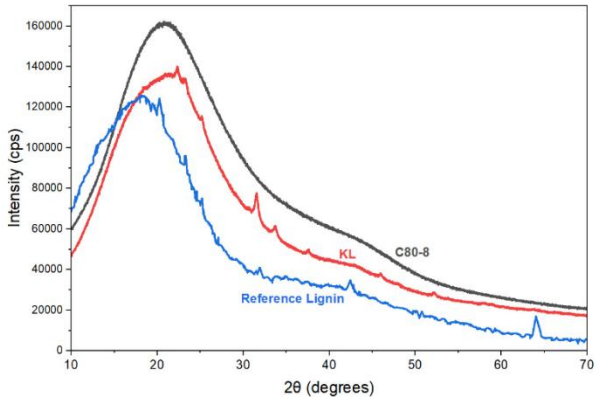


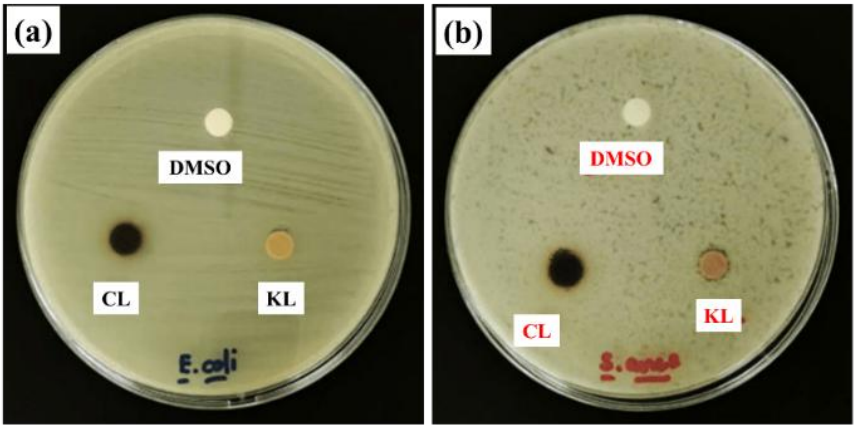
Figure 4 XRD patterns of lignin samples: C80–8 (black), kraft lignin (KL, red), and reference lignin reported by Gomide *et al.* [30] (blue).

Antibacterial activity of lignin

The antibacterial activity of C80–8 lignin (CL) and KL against *E. coli* and *S. aureus* was determined using the disk diffusion method. The inhibition zones in the CL samples were not easily visible due to the dark color of the lignin solution, which prevented direct observation. Nevertheless, the test discs had a larger inhibitory radius than the control. In addition, C80–8 lignin exhibited greater antibacterial activity than KL. The disk diffusion results showed inhibition zone diameters of 8.71 mm against *S. aureus* and 8.31 mm against *E. coli*, while KL showed smaller inhibition zones of 7.88 mm and 7.28 mm, respectively. Although the inhibition zone for KL was clearly visible, its antibacterial effect was comparatively weaker. As shown in **Figures 5(a)** and **5(b)**, the blank control, prepared using the solvent (DMSO) without lignin, exhibited no antibacterial activity against either bacterial strain. These results indicate that lignin possesses antibacterial activity against both Gram-positive and Gram-negative bacteria at the tested concentration.

The antibacterial activity of lignin results from its complex, unique chemical structure, particularly the abundant phenolic hydroxyl and methoxyl groups. These can penetrate and damage bacterial cell membranes, leading to leakage of intracellular components and ultimately cell rupture. Furthermore, lignin molecules with phenolic hydroxyl groups may lower the pH surrounding bacterial cells, resulting in membrane damage. In addition, lignin molecules can generate reactive oxygen species (ROS) that can damage proteins and disrupt the bacterial system. Previous studies on phytochemical-functionalized metal oxide nanomaterials have suggested that ROS generation, particularly superoxide radicals, plays an important role in suppressing microbial growth. For example, Jha *et al.* [31] demonstrated that green-synthesized Ag–Ru/ZnO bimetallic nanocomposites exhibited 99.94% antibacterial activity against *E. coli*

under UV-A irradiation. The antibacterial effect was mainly attributed to oxidative damage to essential cellular components, including DNA, proteins, and lipids, which eventually led to bacterial cell death. These non-specific effects of lignin make it difficult for bacteria to develop resistance to lignin, making it valuable in combating bacterial resistance [6,32]. **Figure 3(b)** shows CL showing relatively higher phenolic-related transmittance intensity than KL, consistent with CL having superior antibacterial ability compared to KL.



Sample	Inhibition zone (mm)	
	E. coli	*S. aureus*
CL	8.31 ± 0.45	8.71 ± 0.42
KL	7.28 ± 0.14	7.88 ± 0.45
Control	6	6

Figure 5 Antibacterial activity of C80–8 lignin (CL) and kraft lignin (KL) against (a) *E. coli* and (b) *S. aureus*, showing the inhibition zones determined by the disk diffusion method.

Furthermore, experimental results indicate that. Lignin appears to exhibit more inhibitory activity against Gram-positive bacteria (*S. aureus*) than against Gram-negative bacteria (*E. coli*), consistent with research by Tran *et al.* [33]. The results showed that all compounds were more effective against the Gram-positive bacterium *S. aureus* than the Gram-negative bacterium *E. coli*. This result can be explained by differences in cell wall structure. Gram-negative bacteria have a thin peptidoglycan layer enclosed by an outer membrane, which acts as a barrier preventing antibacterial agents from easily penetrating. Conversely, Gram-positive bacteria have a thick peptidoglycan layer but lack an outer membrane, allowing the sugar and phenolic components of lignin to directly and effectively adhere to and interact with the Gram-positive bacterial cell wall.

Polymer solution properties

In this study, the polymer properties, including viscosity, conductivity, and surface tension, were investigated to determine the effects of different lignin types and contents in blending with Nylon 6 solutions. As presented in **Table 3**, these properties will determine whether this solution will be formed into filaments in an electrostatic field. The Nylon 6 concentration in the electrospinning solution was fixed at 15% (w/v) in formic acid, while the lignin content ranged from 2.5 to 7.5% (w/w) relative to the weight of Nylon 6. The as-prepared solutions with different compositions appeared as viscous liquids and exhibited slight precipitation after 24 h. This behavior may be attributed to the limited solubility of lignin in formic acid, which has been reported to be approximately 26% (w/w) [34].

The addition of both types of lignin had almost no effect on the surface tension of the solution. In terms of electrical conductivity, it was found that in the initial stage of lignin addition, the conductivity slightly decreased due to the large molecular size of lignin hindering the mobility of charge carriers. However, when the lignin concentration was increased, the conductivity slightly increased again, which was

attributed to the presence of polar functional groups in the lignin structure. This behavior can be explained in accordance with electrohydrodynamic theory, which states that the conductivity of polymer solutions is governed by the type of solvent, polymer structure, and the number of ions in the system [35]. The use of formic acid as a polar solvent promotes the polyelectrolytic behavior of Nylon 6, allowing the structure to dissociate and exhibit sufficiently high initial conductivity to overcome surface tension from the beginning [24].

Table 3 Polymer solution properties of Nylon 6/lignin blends at different lignin concentrations.

Sample	Viscosity (cSt)	Electric conductivity ($mS\ cm^{-1}$)	Surface tension ($mN\ m^{-1}$)
N/L0	65.41 ± 0.30	5.02 ± 0.03	35.47 ± 0.53
N/CL2.5	69.01 ± 0.43	4.73 ± 0.01	35.33 ± 1.05
N/CL5	75.37 ± 0.75	4.76 ± 0.01	36.50 ± 1.37
N/CL7.5	79.88 ± 0.85	4.76 ± 0.01	35.83 ± 0.26
N/KL2.5	54.02 ± 0.12	4.58 ± 0.04	35.82 ± 0.28
N/KL5	54.05 ± 0.54	4.63 ± 0.04	36.16 ± 0.30
N/KL7.5	55.39 ± 0.47	4.79 ± 0.04	35.65 ± 0.32

When the proportion of CL increased, the viscosity of the solution increased (from 65.41 cSt to 79.88 cSt), because of strong intermolecular interactions through the formation of a hydrogen-bonding network between the phenolic hydroxyl groups of lignin and the amide groups of Nylon 6. This is consistent with the findings of Sallem-Idrissi *et al.* [36], who provided clear evidence from FTIR spectra confirming the formation of specific hydrogen bonds between lignin hydroxyl groups and the amine groups of Nylon 6, leading to restricted polymer chain mobility. In addition, Dallmeyer *et al.* [37] further explained the rheological mechanism, indicating that the branched topology structure and the ability of lignin to form associative interactions or hydrogen bonding contribute to a significant increase in solution viscosity.

In contrast, when KL was added, the viscosity of the solution significantly decreased by approximately 15% (down to 54 - 55 cSt). This behavior indicates that KL acts as a plasticizer, inserting itself between Nylon 6 chains, increasing free volume and enhancing chain segment mobility. A study by Park *et al.* [38] demonstrated that plasticization by certain lignin structures can reduce melt/solution viscosity and lower the glass transition temperature (Tg) of the polymer matrix, thereby improving lignin dispersion and flowability. Differences in viscosity behavior reported in previous studies may be related to variations in lignin structure, which depend on both the extraction method and the biomass source [39].

Morphological characterizations

The nanofibers of Nylon 6/CL and Nylon 6/KL blends were obtained using the needleless electrospinning process technique, which is a simple and productive method used to fabricate highly micro- and nanoscale fibers when compared to other technologies [40]. The concentration of lignin in the Nylon 6 solution varies from 0 to 7.5 wt% based on Nylon 6 weight. Each solution was electrospun under the same operational conditions: voltage supply, feeding rate, string-to-collector distance, and relative humidity, as described in the experimental section, and the SEM morphologies of their resulting nanofibers are shown in **Figure 6**.

The average diameters of bead-free electrospun fibers from all samples are shown in **Figure 7**. From the evaluation of the morphological characteristics of nanofibers composed of Nylon 6 blended with CL and KL fabricated by needleless electrospinning, FE-SEM analysis showed that the nanofibers had a relatively uniform structure and smooth surface morphology. Similar characterization approaches using FE-SEM have been widely reported for evaluating the surface morphology of nanomaterials and membrane-based structures [41]. When measuring the fiber diameter and uniformity, it was found that pure Nylon 6 fibers (15 wt%) exhibited a small average diameter of

approximately 43.80 ± 15.97 nm. However, upon the incorporation of lignin into the system, the fiber diameter showed a clear tendency to increase compared to the pure fibers.

In the Nylon 6/CL system, increasing the lignin content generally resulted in an increase in fiber diameter, while the uniformity coefficient decreased. The optimal condition was observed at 5 wt% lignin addition (N/CL5), where the nanofibers exhibited high uniformity, smooth morphology, and an average diameter of 104 nm. A study by Aulova *et al.* [24] which investigated the fabrication of Nylon 6 using a needleless technique, confirmed that fiber diameter is linearly proportional to solution concentration and viscosity. This is consistent with the physical mechanism described by Ojha *et al.* [42], where increasing viscosity enhances chain entanglement density, allowing the jet to better resist stretching forces under an electric field. As a result, bead defects are reduced, and larger, more uniform fibers are formed [12]. The increase in fiber diameter with lignin content is also consistent with the findings of Dallmeyer *et al.* [37], who studied electrospun fibers from technical lignin blended with PEO and reported a similar linear increase in fiber size with increasing concentration. However, when the lignin concentration was increased to 7.5 wt% (N/CL7.5), although the solution exhibited the highest viscosity, the resulting fibers became smaller. This contradictory behavior may be due to the partial precipitation of lignin molecules within the polymer solution, which disrupts jet stability during stretching and leads to non-uniform charge transfer and fiber formation.

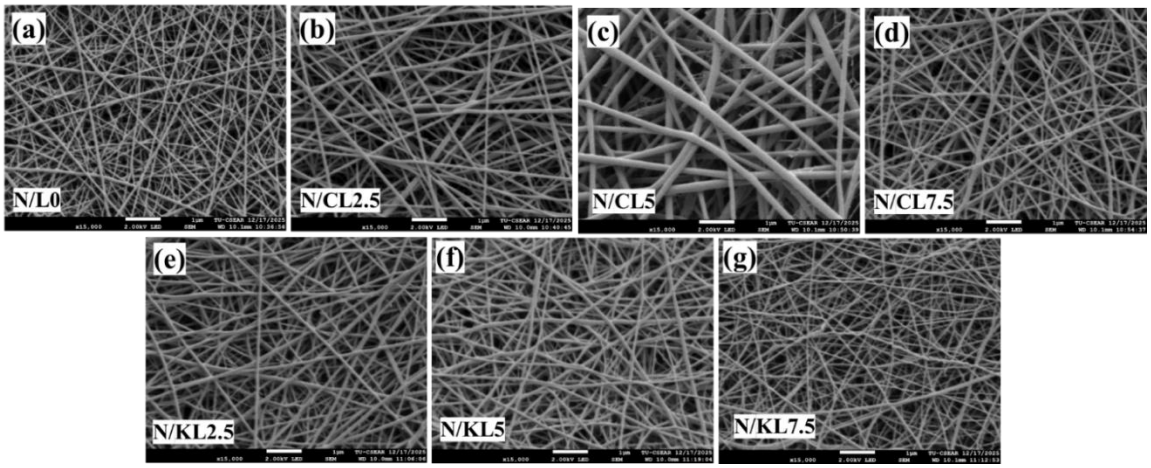


Figure 6 SEM images of the nanofiber mats obtained from the solution of different lignin concentrations: (a) N/L0, (b) N/CL2.5, (c) N/CL5, (d) N/CL7.5, (e) N/KL2.5, (f) N/KL5, and (g) N/KL7.5.

In contrast, increasing the KL content resulted in a decrease in both fiber diameter and uniformity. This behavior is primarily attributed to electrical conductivity. According to Ding *et al.* [43]. An increase in conductivity or charge density in the solution enhances electrostatic repulsion, which results in greater stretching of the polymer jet and the formation of thinner fibers. In addition, it was reported that blending KL reduced the viscosity of the Nylon 6 solution due to its plasticizing effect. According to electrospinning principles, a decrease in viscosity combined with increased conductivity inevitably leads to the formation of thinner fibers [12]. This comparative behavior indicates that the morphology of lignin-based composite fibers is governed by a trade-off between viscosity and conductivity. In the CL system, viscosity is the dominant parameter controlling fiber size, whereas in the KL system, conductivity and reduced flow resistance play a more significant role. Therefore, avoiding lignin content beyond its solubility limit is crucial for maintaining fiber structural integrity [15]. Previous studies have also shown that the addition of extracts or additives does not significantly alter nanofiber morphology, and smooth, bead-free fibers can still be obtained [44].

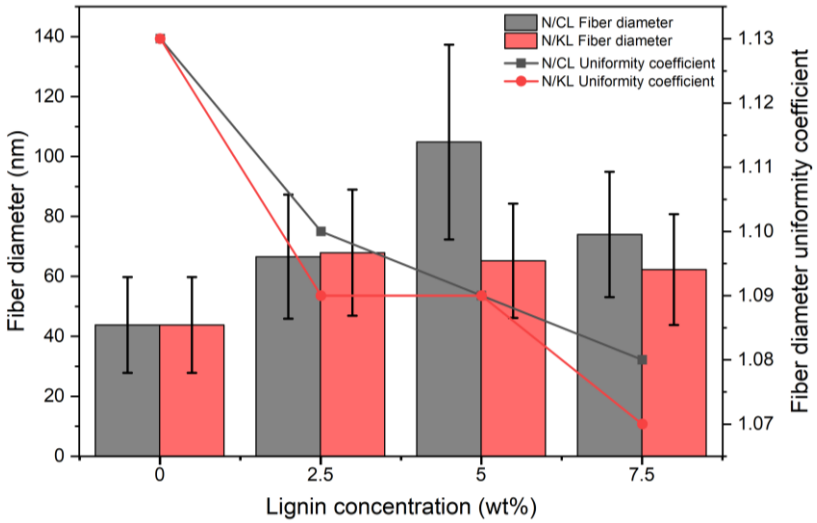


Figure 7 Comparison of the diameters and uniformity coefficient of electrospun fibers prepared from different solutions: Nylon 6, Nylon 6/CL, and Nylon 6/KL at different lignin concentrations (n = 100).

Mechanical properties

The mechanical properties of Nylon 6/lignin fiber mats were evaluated by tensile testing, and the representative stress-strain curves are presented in **Figure 8**. The experimental results show linear elastic behavior of all fiber mats, with no significant permanent deformation before the fracture point. When lignin was incorporated into the Nylon 6 matrix, both the tensile strength and elongation at break increased significantly compared to pure Nylon 6. This observation contradicts the findings of Kai *et al.* [45], which indicates that, according to general polymer blending principles, the addition of lignin typically leads to increased embrittlement of the material due to the rigid three-dimensional structure of lignin. However, the opposite behavior observed in the N/CL system can be explained by the study of Sallem-Idrissi *et al.* [36], who reported the formation of strong and specific hydrogen bonds between the phenolic hydroxyl groups of lignin and the amine/amide groups of Nylon 6. These interactions facilitate effective distribution of stress throughout the fiber network. At the same time, lignin also acts as an internal plasticizer, inserting itself between polymer chains, increasing free volume and chain mobility, thereby enhancing the toughness of the material.

When analyzing the optimal composition, it was found that a lignin content of 5 wt% (N/CL5) represents the optimum loading, providing the highest mechanical performance, with a tensile strength of 5.48 MPa and an elongation at break of 16.62%. In contrast, the use of kraft lignin (N/KL5) resulted in significantly lower strength and toughness due to differences in molecular structure. Kraft lignin undergoes a harsh extraction process that induces condensation reactions, reducing the availability of functional groups [32]. In contrast, CL lignin extracted using green solvents (DES) retains its native structure more effectively, leading to better chemical compatibility with the Nylon 6 matrix. Furthermore, **Table 4** shows that lignin addition also increases Young's modulus (stiffness) by approximately 2.5 - 2.6 times, before decreasing at higher lignin content (7.5 wt%), which is attributed to excessive packing that disrupts polymer chain arrangement and introduces structural defects [46].

The experimental results indicate that fiber mats composed of smaller-diameter fibers exhibit lower Young's modulus and elongation, whereas larger fibers can withstand greater stress and deformation, which can be explained by the model proposed by Pai *et al*. [47]. This model states that the mechanical properties of fiber mats are not governed solely by intrinsic material properties but are strongly influenced by fiber curvature and junction distance. Submicron fibers typically exhibit high curvature due to the electrospinning process, causing most of the applied energy under tensile loading to be consumed in unbending before actual load occurs. As a result, fiber mats composed of smaller fibers exhibit lower overall modulus and elongation compared to those composed of larger fibers.

Table 3 Tensile properties of electrospun Nylon 6/lignin nanofiber mats as a function of lignin content.

Sample	Tensile strength (MPa)	Elongation at break (%)	Young's Modulus (MPa)
N/L0	1.52 ± 1.05	10.18 ± 3.89	79.28 ± 8.26
N/CL2.5	5.09 ± 0.47	12.51 ± 1.70	205.26 ± 4.60
N/CL5	5.48 ± 0.76	16.62 ± 4.91	173.76 ± 8.49
N/CL7.5	3.92 ± 1.08	14.75 ± 3.48	141.67 ± 13.16
N/KL2.5	5.52 ± 0.84	13.87 ± 3.15	201.96 ± 4.74
N/KL5	4.17 ± 0.84	13.20 ± 1.96	163.70 ± 10.62
N/KL7.5	3.92 ± 0.71	12.48 ± 2.50	158.65 ± 4.89

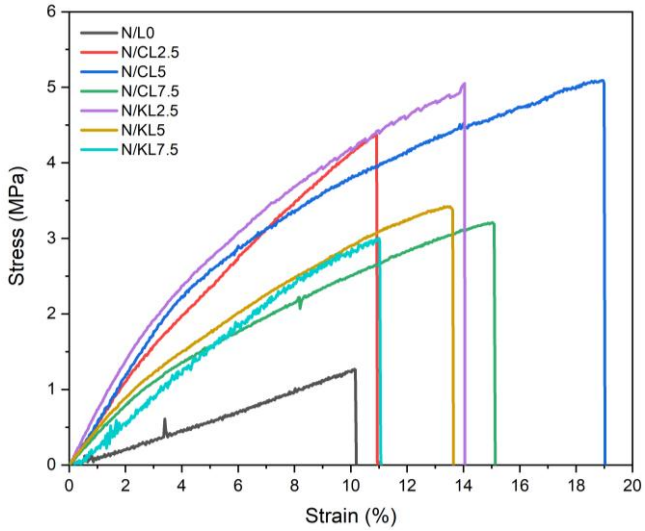


Figure 8 Tensile stress-strain curves of Nylon 6/lignin nanofiber mats by uniaxial stretching.

Antibacterial activity of the nanofiber mats

The inhibition zones presented in **Figure 9** show the results of the antibacterial efficacy testing of lignin-infused Nylon 6 nanofiber mats. The research found that both types of lignin-infused nanofiber mats (CL and KL) exhibited significantly better antibacterial activity against Gram-positive bacteria (*S. aureus*) than against Gram-negative bacteria (*E. coli*). Pure Nylon 6 showed no antibacterial activity. This antibacterial efficacy varied with increasing lignin content. The highest efficacy was observed at 5 wt% of lignin doping, but as the lignin content increased to 7.5 wt%, the antibacterial activity decreased to the point of being undetectable. This is consistent with the smaller fiber diameter under these conditions, a limitation that hinders the release of phenolic hydroxyl groups to react with bacteria. Moreover, the nanofibers infused with CL demonstrated greater effectiveness than KL, which can be attributed to the completeness of their chemical structure. Research by Alzagameem *et al.* [14] reported that the antimicrobial activity of lignin is due to the amount of phenolic hydroxyl and methoxyl groups in its structure. These functional groups can interfere with the stability of bacterial cell membranes and induce oxidative stress through the generation of reactive oxygen species, leading to leakage of intracellular components and ultimately cell death. Lignin extracted with DES solvent preserves these functional groups better. The lack of inhibitory activity against *E. coli* under all conditions is hypothesized by the researchers to be insufficient in the amount of lignin used to disrupt the structure of gram-negative bacteria. The superior activity of Nylon 6/lignin nanofibers against *S. aureus* compared to *E. coli* is due to their different cell wall structures. Gram-

negative bacteria like *E. coli* have an outer membrane composed of lipopolysaccharides, which acts as a strong barrier against the penetration of antimicrobial agents, making gram-positive bacteria more susceptible to polyphenolic compounds [48]. This information is consistent with the research by Nekooei and Ajji [13], who developed alkali-lignin-infused PET nanofibers, indicating that complete inhibition of *E. coli* requires specific lignin-based nanofibers. A high lignin content of up to 15 - 20 wt% is required in the matrix, which clearly explains why the 5 - 7.5 wt% lignin content in this research was insufficient to inhibit the bacteria.

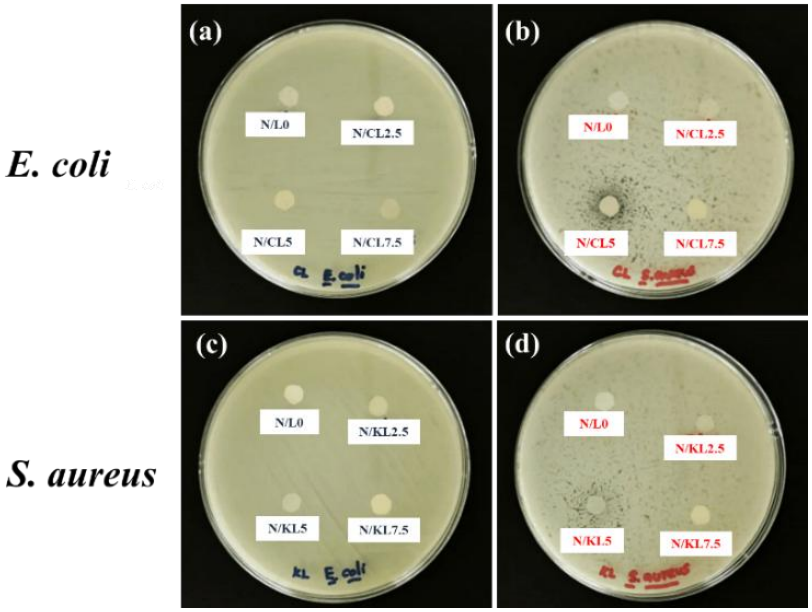


Figure 1 Inhibition zones obtained by the disk diffusion method for pure Nylon 6 and lignin-containing Nylon 6/CL and Nylon 6/KL nanofiber mats with varying lignin contents against *E. coli* (a, b) and *S. aureus* (c, d).

Research by Ryšánek *et al.* [49] Studying Nylon 6 nanofibers confirms that pure Nylon 6 polymer does not possess inherent antibacterial properties. The bioactivity of the fiber sheets relies on the release of substances into the environment, as shown in the research of Charernsriwilaiwat *et al.* [50], which indicates that the antimicrobial mechanism from nanofibers occurs effectively when the active ingredients can diffuse from the fiber matrix into the bacterial solution. The excessively small fiber size may cause lignin molecules to be tightly bound or encapsulated within the polymer matrix, resulting in reduced reaction and hindering the release of phenolic hydroxyl groups to destroy bacteria.

Conclusions

In this study, lignin was successfully extracted from coconut coir using a DES system under optimized conditions (80 °C, 8 h; C80–8), which yielded the highest extraction efficiency and the lowest IC_{50} value, indicating superior antioxidant activity among the investigated conditions. Notably, C80–8 also exhibited a larger antibacterial inhibition zone than KL. FTIR analysis confirmed that the DES process can fully preserve the important functional groups of lignin in its native state. To support this conclusion, Chen *et al.* [10]. Clearly stated that DES is a green solvent with low toxicity and high thermal stability, which not only effectively dissolves lignin from biomass but also provides chemical dynamics favorable for lignin valorization.

In the fabrication step, the study successfully incorporated the extracted lignin into a Nylon 6 polymer matrix to produce nanofiber mats via needleless electrospinning. The optimal composition was found at 5 wt% lignin loading (N/CL5), which resulted in highly uniform nanofibers (average diameter of 104 nm) and increased Young's modulus, indicating improved stiffness and efficient stress transfer, reflecting enhanced mechanical properties. This enhancement results from hydrogen bonding between lignin and Nylon 6, improving stress distribution and reducing material brittleness [36] while Nylon 6 serves as an

effective matrix for bio-based nanomaterials [49]. The N/CL5 nanofiber mats displayed notable antibacterial activity, especially against Gram-positive bacteria, such as *Staphylococcus aureus*. Additionally, the incorporation of lignin into the electrospun fiber network aligns with the findings of Nekooei and Ajji [13], who demonstrated the potential of these materials for use as filtration membranes that can inhibit both bacteria and viruses.

This study provided evidence that combining DES-based lignin extraction with needleless electrospinning was an eco-friendly and scalable approach, converting agricultural waste such as coconut coir into valuable nanofiber materials.

Acknowledgements

The authors acknowledge funding from the Faculty of Engineering, Thammasat School of Engineering, and the research unit in polymer rheology and processing at Thammasat University, Pathumthani 12120, Thailand.

Declaration of generative AI in scientific writing

The authors acknowledge the use of generative AI tools (e.g., Grammarly and ChatGPT by OpenAI) in the preparation of this manuscript, specifically for language editing and grammar correction. AI performed no content generation or data interpretation. The authors take full responsibility for the content and conclusions of this work.

CRediT author statement

Supapohn Pohnanothai: Conceptualization, Methodology, Investigation, Data curation, Formal analysis, Visualization, Writing - original draft. **Patcharaporn Wutticharoenmongkol:** Conceptual-ization, Validation, Supervision, Writing -review & editing, Project administration, Funding acquisition.

References

[1] T Kalak. Potential use of industrial biomass waste as a sustainable energy source in the future. *Energies* 2023; **16(4)**, 1783.

[2] M Nissar, KN Chethan, YA Birjerane, S Patil, S Shetty and A Das. Coconut coir fiber composites for sustainable architecture: A comprehensive review of properties, processing, and applications. *Journal of Composites Science* 2025; **9(10)**, 516.

[3] F Vieira, HEP Santana, M Jesus, J Santos, P Pires, M Vaz-Velho, DP Silva and DS Ruzene. Coconut waste: Discovering sustainable approaches to advance a circular economy. *Sustainability* 2024; **16(7)**, 3066.

[4] D Watkins, M Nuruddin, M Hosur, A Tcherbi-Narteh and S Jeelani. Extraction and characterization of lignin from different biomass resources. *Journal of Materials Research and Technology* 2015; **4(1)**, 26-32.

[5] H Sadeghifar and A Ragauskas. Lignin as a UV light blocker—a review. *Polymers* 2020; **12(5)**, 1134.

[6] AK Das, K Mitra, AJ Conte, A Sarker, A Chowdhury and AJ Ragauskas. Lignin-A green material for antibacterial application—A review. *International Journal of Biological Macromolecules* 2024; **261(2)**, 129753.

[7] M Joshi and S Manjare. Chemical approaches for the biomass valorisation: A comprehensive review of pretreatment strategies. *Environmental Science and Pollution Research* 2024; **31**, 48928-48954.

[8] AK Tamo, I Doench, G Deffo, SLZ Jiokeng, G Doungmo, CG Fotsop, RCT Temgoua, A Montembault, A Serghei, E Njanja, IK Tonle and A Osorio-Madrazo. Lignocellulosic biomass and its main structural polymers as sustainable materials for (bio)sensing applications. *Journal of Materials Chemistry A* 2025; **13(30)**, 24185-24253.

[9] Z Yao, G Chong and H Guo. Deep eutectic solvent pretreatment and green separation of lignocellulose. *Applied Sciences* 2024; **14(17)**, 7662.

[10] Z Chen, A Ragauskas and C Wan. Lignin extraction and upgrading using deep eutectic solvents. *Industrial Crops and Products* 2020; **147**, 112241.

[11] BAV Maran, S Jeyachandran and M Kimura. A review on the electrospinning of polymer nanofibers and its biomedical applications. *Journal of Composites Science* 2024; **8(1)**, 32.

[12] A Al-Abduljabbar and I Farooq. Electrospun polymer nanofibers: Processing, properties, and applications. *Polymers* 2023; **15(1)**, 65.

[13] A Nekooei and A Ajji. Integrating alkali lignin into electrospun PET nanofibers for enhanced viral protection in respiratory masks. *ACS Omega* 2026; **11(4)**, 6500-6512.

[14] A Alzagameem, SE Klein, M Bergs, XT Do, I Korte, S Dohlen, C Hüwe, J Kreyenschmidt, B Kamm, M Larkins and M Schulze. Antimicrobial activity of lignin and lignin-derived cellulose and chitosan composites against selected pathogenic and spoilage microorganisms. *Polymers* 2019; **11(4)**, 670.

[15] V Raja, L Mahalakshmi, MM Leena, JA Moses and C Anandharamakrishnan. Needleless electrospinning: Concepts and applications in the food industry. *Food Engineering Reviews* 2024; **16**, 252-269.

[16] OE Fayemi, PB Letsholo, HO Shoyiga, CC Ahia and EL Meyer. Investigation of the effects of concentration and voltage on the physicochemical properties of Nylon 6 nanofiber membrane. *Scientific Reports* 2025; **15**, 10865.

[17] A Isci and M Kaltschmitt. Recovery and recycling of deep eutectic solvents in biomass conversions: A review. *Biomass conversion and biorefinery* 2022; **12(1)**, 197-226.

[18] EA Agustiany, MR Ridho, M Rahmi D N, EW Madyaratri, F Falah, MAR Lubis, NN Solihat, FA Syamani, P Karungamye, A Sohail, DS Nawawi, AH Prianto, AH Iswanto, M Ghozali, WK Restu, I Juliana, P Antov, L Kristak, W Fatriasari and A Fudholi. Recent developments in lignin modification and its application in lignin-based green composites: A review. *Polymer Composites* 2022; **43(8)**, 4848-4865.

[19] AK Kumar, BS Parikh and M Pravakar. Natural deep eutectic solvent mediated pretreatment of rice straw: Bioanalytical characterization of lignin extract and enzymatic hydrolysis of pretreated biomass residue. *Environmental science and pollution research* 2016; **23**, 9265-9275.

[20] J Rencoret, J Ralph, G Marques, A Gutiérrez, AT Martínez and JC del Río. Structural characterization of lignin isolated from coconut (*Cocos nucifera*) coir fibers. *Journal of Agricultural and Food Chemistry* 2013; **61(10)**, 2434-2445.

[21] J Rumpf, R Burger and M Schulze. Statistical evaluation of DPPH, ABTS, FRAP, and Folin-Ciocalteu assays to assess the antioxidant capacity of lignins. *International Journal of Biological Macromolecules* 2023; **233**, 123470.

[22] N Jadid, D Hidayati, SR Hartanti, BA Arraniry, RY Rachman and W Wikanta. Antioxidant activities of different solvent extracts of *Piper retrofractum* Vahl. using DPPH assay. *AIP conference proceedings* 2017; **1845(1)**, 020019.

[23] O Gordobil, R Herrera, M Yahyaoui, S İlk, M Kaya and J Labidi. Potential use of kraft and organosolv lignins as a natural additive for healthcare products. *RSC advances* 2018; **8(43)**, 24525-24533.

[24] A Aulova, M Bek, L Kossovich and I Emri. Needleless electrospinning of PA6 fibers: The effect of solution concentration and electrospinning voltage on fiber diameter. *Strojniski Vestnik Journal of Mechanical Engineering* 2020; **66(7-8)**, 421-430.

[25] FC Çallıoğlu and HK Güler. Production of essential oil-based composite nanofibers by emulsion electrospinning. *Pamukkale Üniversitesi Mühendislik Bilimleri Dergisi* 2020; **26(7)**, 1178-1185.

[26] AR Mankar, A Pandey and KK Pant. Microwave-assisted extraction of lignin from coconut coir using deep eutectic solvents and its valorization to aromatics. *Bioresource Technology* 2022; **345**, 126528.

[27] X Duan, X Wang, J Chen, G Liu and Y Liu. Structural properties and antioxidation activities of lignins isolated from sequential two-step formosolv fractionation. *RSC advances* 2022; **12(37)**, 24242-24251.

[28] A Alzagameem, BE Khaldi-Hansen, D Büchner, M Larkins, B Kamm, S Witzleben and M Schulze. Lignocellulosic biomass as source for lignin-based environmentally benign antioxidants. *Molecules* 2018; **23(10)**, 2664.

[29] D Agrawal, A Tripathi, P Pal, M Hoque, SD Bharathi and S Jacob. Sustainable extraction strategy for lignin from coconut coir using organosolv and deep eutectic solvents (DES). *Waste and Biomass Valorization* 2025; **16**, 1599-1608.

[30] RAC Gomide, ACS de Oliveira, DAC Rodrigues, CR de Oliveira, OBG de Assis, MV Dias and SV Borges. Development and characterization of lignin microparticles for physical and antioxidant enhancement of biodegradable polymers. *Journal of Polymers and the Environment* 2020; **28**, 1326-1334.

[31] PK Jha, T Jaidumrong, D Rokaya and C Ovatlarnporn. *Callistemon viminalis* leaf extract phytochemicals modified silver-ruthenium bimetallic zinc oxide nanocomposite biosynthesis: Application on nanocoating photocatalytic *Escherichia coli* disinfection. *RSC advances* 2024; **14(16)**, 11017-11026.

[32] JL Espinoza-Acosta, PI Torres-Chávez, B Ramírez-Wong, CM López-Saiz and B Montaño-Leyva. Antioxidant, antimicrobial, and antimutagenic properties of technical lignins and their applications. *BioResources* 2016; **11(2)**, 5452-5481.

[33] NT Tran, TTT Nguyen, D Ha, TH Nguyen, NN Nguyen, K Baek, NT Nguyen, CK Tran, TTV Tran and HV Le. Highly functional materials based on nano-lignin, lignin, and lignin/silica hybrid capped silver nanoparticles with antibacterial activities. *Biomacromolecules* 2021; **22(12)**, 5327-5338.

[34] T Rashid, CF Kait, I Regupathi and T Murugesan. Dissolution of kraft lignin using protic ionic liquids and characterization. *Industrial Crops and Products* 2016; **84**, 284-293.

[35] S Ghosh and K Pramanik. A comprehensive review on lignin based electrospun nanomaterials as suitable adsorbents for remediation of Detrimental Water and Air Pollutants. *Water, Air, & Soil Pollution* 2024; **235**, 485.

[36] N Sallem-Idrissi, M Sclavons, DP Debecker and J Devaux. Miscible raw lignin/nylon 6 blends: Thermal and mechanical performances. *Journal of Applied Polymer Science* 2015; **133(6)**, 42963.

[37] I Dallmeyer, F Ko and JF Kadla. Electrospinning of technical lignins for the production of fibrous networks. *Journal of Wood Chemistry and Technology* 2010; **30(4)**, 315-329.

[38] CW Park, WJ Youe, SJ Kim, SY Han, JS Park, EA Lee, GJ Kwon, YS Kim, NH Kim and SH Lee. Effect of lignin plasticization on physico-mechanical properties of lignin/poly (Lactic acid) composites. *Polymers* 2019; **11(12)**, 2089.

[39] D Kun and B Pukánszky. Polymer/lignin blends: Interactions, properties, applications. *European Polymer Journal* 2017; **93**, 618-641.

[40] M Kumar, M Hietala and K Oksman. Lignin-based electrospun carbon nanofibers. *Frontiers in Materials* 2019; **6**, 62.

[41] MS Jamal, MS Chowdhury, S Bajgai, M Hossain, A Laref, PK Jha and K Techato. Comparative studies on the morphological, structural and optical properties of NiO thin films grown by vacuum and non-vacuum deposition techniques. *Materials Research Express* 2021; **8**, 126404.

[42] S. S. Ojha, M. Afshari, R. Kotek and R. E. Gorga. Morphology of electrospun nylon-6 nanofibers as a function of molecular weight and processing parameters. *Journal of applied polymer science* 2008; **108(1)**, 308-19.

[43] R Ding, H Wu, M Thunga, N Bowler and MR Kessler. Processing and characterization of low-cost electrospun carbon fibers from organosolv lignin/polyacrylonitrile blends. *Carbon* 2016; **100**, 126-136.

[44] G Ajith, GP Tamilarasi, G Sabarees, S Gouthaman, K Manikandan, V Velmurugan, V Alagarsamy and VR Solomon. Recent developments in electrospun nanofibers as delivery of phytoconstituents for wound healing. *Drugs and Drug Candidates* 2023; **2(1)**, 148-171.

[45] D Kai, S Jiang, ZW Low and XJ Loh. Engineering highly stretchable lignin-based electrospun nanofibers for potential biomedical applications. *Journal of Materials Chemistry B* 2015; **3(30)**, 6194-6204.

[46] MR Ridho, EA Agustiany, MR Dn, EW Madyaratri, M Ghozali, WK Restu, F Falah, MAR Lubis, FA Syamani, Y Nurhamiyah, S Hidayati, A Sohail, P Karungamye, DS Nawawi, AH Iswanto, N Othman, NAM Aini, MH Hussin, K Sahakaro, N Hayeemasae, ..., W Fatriasari. Lignin as green filler in polymer composites: Development methods, characteristics, and potential applications. *Advances in Materials Science and Engineering* 2022; **2022(1)**, 1363481.

[47] CL Pai, MC Boyce and GC Rutledge. On the importance of fiber curvature to the elastic moduli

of electrospun nonwoven fiber meshes. *Polymer* 2011; **52(26)**, 6126-6133.

[48] Y He, HC Ye, TT You and F Xu. Sustainable and multifunctional cellulose-lignin films with excellent antibacterial and UV-shielding for active food packaging. *Food Hydrocolloids* 2023; **137**, 108355.

[49] P Ryšánek, M Malý, P Čapková, M Kormunda, Z Kolská, M Gryndler, O Novák, L Hocelíková, L Bystrianský and M Munzarová. Antibacterial modification of nylon-6 nanofibers: Structure, properties and antibacterial activity. *Journal of Polymer Research* 2017; **24**, 208.

[50] N Charernsriwilaiwat, T Rojanarata, T Ngawhirunpat, M Sukma and P Opanasopit. Electrospun chitosan-based nanofiber mats loaded with *Garcinia mangostana* extracts. *International journal of pharmaceutics* 2013; **452(1-2)**, 333-343.